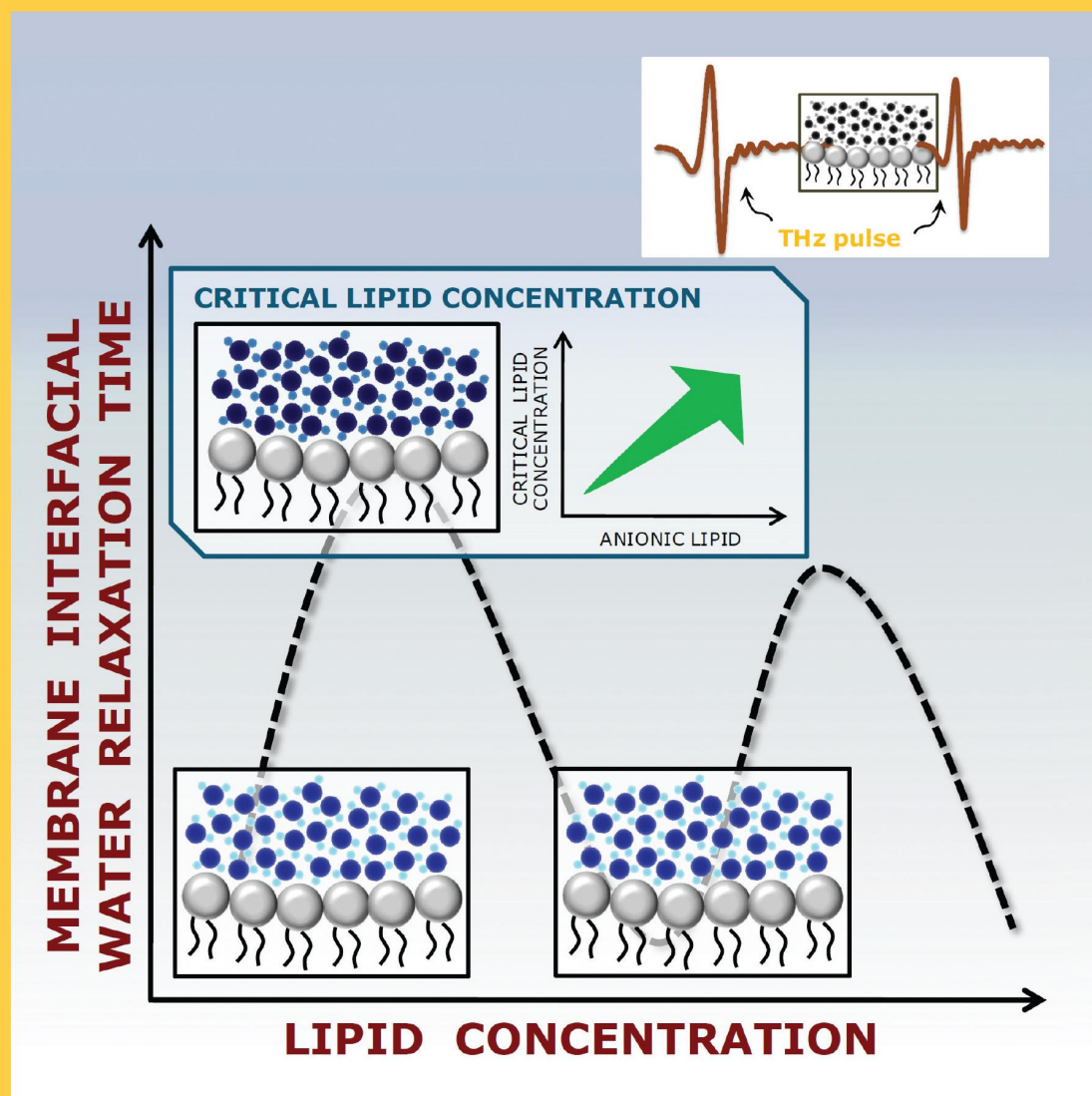


THE JOURNAL OF PHYSICAL CHEMISTRY

B



Phospholipid
Headgroup Charge as
a Key Determinant in
Membrane Interfacial
Water Dynamics

BIOPHYSICAL CHEMISTRY, BIOMATERIALS, LIQUIDS, AND SOFT MATTER



ACS Publications
Most Trusted. Most Cited. Most Read.

www.acs.org

Effect of Phospholipid Headgroup Charge on the Structure and Dynamics of Water at the Membrane Interface: A Terahertz Spectroscopic Study

Sreetama Pal,^{‡,§,||} Nirnay Samanta,^{||,⊥} Debasish Das Mahanta,^{||} Rajib Kumar Mitra,^{*,||} and Amitabha Chattopadhyay^{*,†,‡,§}

[†]CSIR-Centre for Cellular and Molecular Biology, Uppal Road, Hyderabad 500 007, India

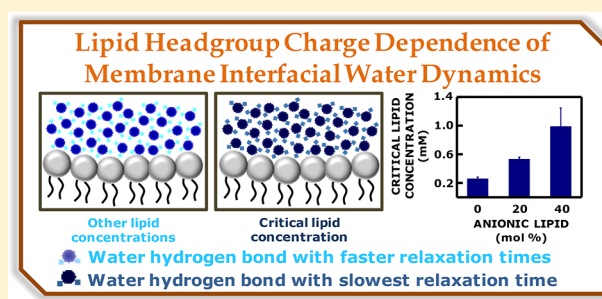
[‡]Academy of Scientific and Innovative Research, India

[§]CSIR-Indian Institute of Chemical Technology, Uppal Road, Hyderabad 500 007, India

^{||}S.N. Bose National Centre for Basic Sciences, Block JD, Sector III, Salt Lake, Kolkata 700 106, India

Supporting Information

ABSTRACT: Biological membranes are highly organized supra-molecular assemblies of lipids and proteins. The membrane interface separates the outer (bulk) aqueous phase from the hydrophobic membrane interior. In this work, we have explored the microstructure and collective dynamics of the membrane interfacial hydration shell in zwitterionic and negatively charged phospholipid membrane bilayers using terahertz time-domain spectroscopy. We show here that the relaxation time constants of the water hydrogen bond network exhibit a unique “rise and dip” pattern with increasing lipid concentration. More importantly, we observed a dependence of the critical lipid concentration corresponding to the inflection point on the charge of the lipid headgroup, thereby implicating membrane electrostatics as a major factor in the microstructure and dynamics of water at the membrane interface. These results constitute one of the first experimental evidences of the modulation of the dielectric relaxation response of membrane interfacial water by membrane lipid composition in a concentration-dependent manner. Lipid-stringent membrane hydration could be relevant in the broader context of lipid diversity observed in biological membranes and the role of negatively charged lipids in membrane protein structure and function.



INTRODUCTION

Biological membranes are highly organized *quasi* two-dimensional supramolecular self-assemblies of lipids and proteins. Membranes can be physically treated as deformable, anisotropic “soft matter”.^{1,2} The formation of membranes, an essential evolutionary prerequisite for biological compartmentalization,³ is ascribed to the hydrophobic effect.^{4,5} The hydrophobic effect is a manifestation of the strong attractive forces between water molecules, that levies an entropic penalty to the incorporation of nonpolar molecules in an aqueous environment and leads to their exclusion from the immediate vicinity of the solvent. Contrary to earlier textbook representations of the membrane as a static, isotropic, low dielectric hydrocarbon “slab” surrounded by polar lipid headgroups and water, biological membranes are now represented by a dynamic and chemically heterogeneous environment along the membrane normal (see Figure 1a).^{6,7} As a direct consequence of this dynamic heterogeneity, the membrane interface, operationally defined as the effective depth of water penetration (~ 15 Å in thickness in fluid phosphatidylcholine membranes), is not sharply defined

and is modulated by temperature, hydration, and lipid chemistry.⁸

The membrane interface (see Figure 1a) ensures a dynamic segregation of the bulk (outer) aqueous phase from the more isotropic, hydrophobic membrane core and exhibits distinct chemical, motional, and dielectric signatures.⁹ This region, owing to its unique physicochemical properties, plays a crucial role in modulating biochemical processes such as substrate recognition and function of membrane-active enzymes.^{10–12} At a molecular level, the membrane interface imposes a dynamic spatiotemporal confinement on water molecules due to reduced probability of energetically favorable hydrogen bonding induced by geometrical constraints.¹³ As a result, the membrane interface displays slow rates of solvent relaxation⁶ and is involved in intermolecular charge interactions¹⁴ and hydrogen bonding mediated by polar phospholipid headgroups.^{15,16}

Received: February 15, 2018

Revised: March 6, 2018

Published: March 15, 2018

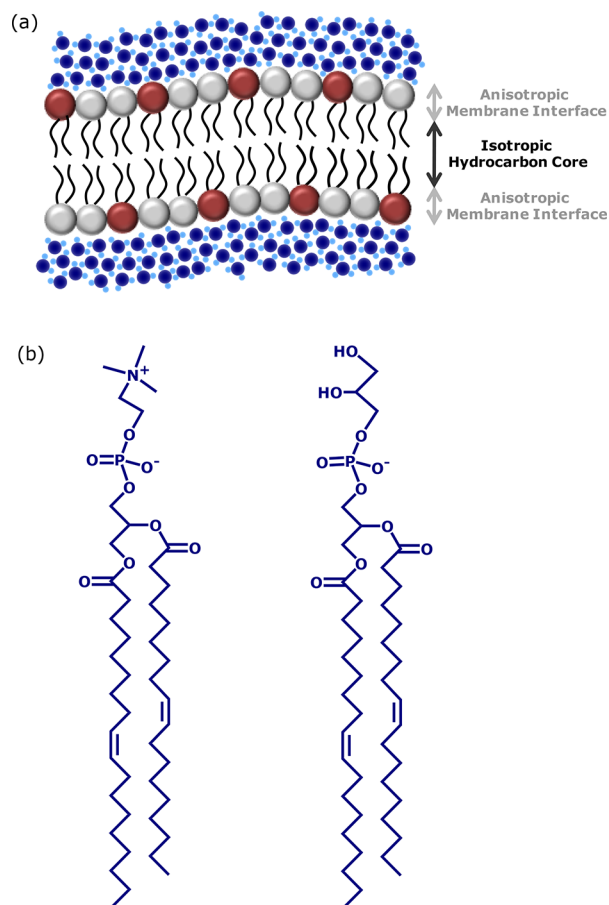


Figure 1. (a) Schematic representation of a hydrated membrane bilayer showing the highly structured, dynamic hydrogen bond network of interfacial water. Zwitterionic phospholipid headgroups are depicted as gray beads, whereas those with anionic headgroups are represented as maroon beads. The phospholipid fatty acyl chains are shown in black. Water molecules are depicted in blue, with the darker shade corresponding to the oxygen atom and the lighter shade corresponding to the two hydrogen atoms. The anisotropic membrane interface is characterized by restricted dynamics and connects the outer (bulk) aqueous phase to the hydrophobic (hydrocarbon-like) membrane interior. (b) Chemical structures of representative phospholipids: zwitterionic DOPC (left) and anionic DOPG (right) at neutral pH. Lipids with a phosphatidylcholine (PC) headgroup represent predominant membrane lipids in eukaryotic cells. Lipids with a negatively charged phosphatidylglycerol (PG) headgroup are crucial in lipid–protein interactions. See text for more details.

Work from a number of laboratories has established the emerging role of hydration as an essential regulatory mechanism for a variety of biomolecular interactions. In particular, water plays an important role in the structure, function, and dynamics of organized biological assemblies such as membranes.^{17–19} Water molecules are known to mediate lipid–protein interactions and function of membrane proteins. The presence of ordered water molecules has proven to be a common feature in the crystal structure of many membrane proteins.²⁰ Interestingly, water has been shown to act as a “foldase” by catalyzing the exchange of hydrogen bonds during the protein folding process.²¹ We have previously shown that the extent of dynamic constraint imposed by proteins and peptides on neighboring water molecules could be used as a marker for protein structure and function.^{6,22–24}

Previous studies on organization and dynamics of membrane interfacial water utilized experimental approaches such as infrared,²⁵ fluorescence,¹⁷ and pump–probe²⁶ spectroscopy and X-ray and neutron diffraction.^{27,28} Terahertz (THz) spectroscopy ($1 \text{ THz} = 10^{12} \text{ Hz} = 1 \text{ ps}^{-1}$) is a powerful tool for label-free and noninvasive determination of the collective low energy intermolecular vibrations of the hydrogen bond network of water, otherwise inaccessible to conventional spectroscopic techniques.^{29–32} THz spectroscopy is particularly well suited for investigation of hydration dynamics in biological systems due to its unprecedented sensitivity and non-ionizing properties. The THz regime is associated with the dynamic reorganization of the water hydrogen bond network around the solute, which usually consists of several hydration shells.^{33–35} In addition, terahertz time-domain spectroscopy (THz-TDS) offers the advantage of simultaneous measurement of both the phase and amplitude of the transmitted THz radiation, thereby enabling the quantitation of various optical parameters (such as absorption coefficients, complex refractive indexes, and complex dielectric constants) by numerically solving Fresnel’s transmittance equations.²⁹

The functional relevance of membrane interfacial water in complex biological processes is only beginning to be addressed. In this overall context, with the objective of delineating the role of membrane electrostatics on the water hydrogen bond network, we have explored the microstructure and collective dynamics of the extended hydration sheath of water at the interface of membrane bilayers of varying lipid composition (and interfacial charge) using THz-TDS. Our results indicate that surface electrostatics and steric crowding are key players in dictating the organization and dynamics of water molecules at the membrane interface. The lipid stringency in membrane hydration assumes relevance in the context of the lipid diversity observed in biological membranes³⁶ and the regulatory role of negatively charged lipids in a variety of membrane-associated phenomena.^{37–39}

■ EXPERIMENTAL SECTION

Materials. 1,2-Dioleoyl-*sn*-glycero-3-phosphocholine (DOPC) and 1,2-dioleoyl-*sn*-glycero-3-phosphoglycerol (DOPG) lipids (see Figure 1b) were acquired from Avanti Polar Lipids (Alabaster, AL). 1,2-Dimyristoyl-*sn*-glycero-3-phosphocholine (DMPC) was from Sigma Chemical Co. (St. Louis, MO). Thin layer chromatography in chloroform/methanol/water (65:35:5, v/v/v) was utilized to check lipid purity. Silica gel precoated plates obtained from Merck (Darmstadt, Germany) were used for this purpose. Lipids were visualized by charring with a solution containing cupric sulfate (10%, w/v) and phosphoric acid (8%, v/v) at $\sim 150 \text{ }^\circ\text{C}$ ⁴⁰ and gave a single spot in all cases. Phospholipids were digested by perchloric acid, and their concentration was subsequently determined by phosphate assay.⁴¹ The extent of lipid digestion was assessed by using DMPC as an internal standard. All other chemicals used were of the highest purity available. Water purified through a Millipore (Bedford, MA) Milli-Q system and spectroscopic grade solvents were used throughout.

Preparation of Lipid Vesicles. Large unilamellar vesicles (LUVs) of $\sim 100 \text{ nm}$ diameter of DOPC, DOPC/DOPG (80/20, mol/mol), or DOPC/DOPG (60/40, mol/mol) were utilized for all experiments. The lipid concentrations studied ranged from 0.1 to 4 mM. For LUV preparation, lipids (DOPC or DOPC/DOPG) were mixed well (in the case of binary mixtures) and dried by gentle warming ($\sim 35 \text{ }^\circ\text{C}$) under a

stream of nitrogen. Subsequently, the lipid mixture was further dried under a high vacuum for at least 3 h and hydrated (swelled) by addition of 50 mM phosphate buffer (pH 7.0). A uniform dispersion (homogenization) of lipids in the multilamellar vesicles (MLVs) formed at this step was ensured by intermittent vortexing of each sample for ~ 3 min. These MLVs were then freeze–thawed five times using liquid nitrogen and a water bath maintained at ~ 50 °C to ensure solute equilibration between trapped and bulk solution. Subsequently, the homogenized and solute equilibrated MLVs were extruded through polycarbonate filters (with a pore diameter of 100 nm) mounted in an Avanti Liposofast Extruder (Avanti Polar Lipids, Alabama, AL) fitted with Hamilton syringes (Hamilton Company, Reno, NV). Samples were subjected to at least 11 passes through the polycarbonate filters to give the final LUV suspension. Details of the extrusion technique employed have been described elsewhere.⁴² Samples were incubated for 12 h at room temperature (~ 23 °C) for equilibration prior to data acquisition.

THz-TDS Setup. A commercially available THz spectrophotometer, TERA K8 (Menlo System, Martinsried, Germany), was used for THz-TDS measurements. The details of the spectrometer could be found elsewhere.^{43,44} A 780 nm Er doped fiber laser of very short pulse width (~ 100 fs) and a 100 MHz repetition rate was used to excite a THz emitter photo conducting (PC) antenna, thereby generating a THz radiation characterized by a bandwidth of up to 3 THz. This THz radiation was focused on the sample, and a similar PC antenna, gated by the coherent probe laser beam, was used to detect the transmitted THz radiation. Both of the PC antennas consist of gold dipoles deposited on low temperature grown GaAs substrate, with a dipole gap of 5 μm . To avoid interference from water vapor absorption, a dry nitrogen atmosphere with a controlled humidity of $<10\%$ was maintained during the data acquisition. All measurements were carried out at ~ 20 °C. A cell (Bruker, model A 145) with z-cut quartz windows and a Teflon spacer of 100 μm thickness, in which the sample was injected, was used for the measurements. For each sample, three observations were averaged together to minimize error.

Data Analysis and Interpretation. THz-TDS measurements utilize the reduction in amplitude and temporal shift of the THz pulse in the presence of samples (lipid vesicles, in this case) to quantitate different optical parameters associated with the sample.^{45,46} The amplitude ($E_{\text{THz}}(t)$) and phase of the THz electric field for each sample were measured as a function of time by inducing a wide range of temporal delay between the probe and the pump beam. The obtained time domain information was converted to a frequency domain by a fast Fourier transform (FFT) algorithm for ease of data handling and subsequent analysis. The THz-TDS data was analyzed using the TeraLyzer software (www.lytera.com) to extract information about optical parameters, e.g., absorption coefficient (α), refractive index (n), and complex dielectric constant ($\tilde{\epsilon}$), characteristic of the sample. The relevant equations have been included elsewhere (see the [Results and Discussion](#) and [section S1](#)). The extracted frequency-dependent complex dielectric constants for lipid samples of various compositions at each concentration were then deconvoluted with a Debye model^{44,47–55} to obtain information about the dynamics of water molecules at the membrane interface.

According to the Debye model, the frequency-dependent complex dielectric response of membrane interfacial water can be described as

$$\tilde{\epsilon}(\nu) = \epsilon_{\infty} + \sum_{j=1}^m \frac{\epsilon_j - \epsilon_{j+1}}{1 + i2\pi\nu\tau_j} \quad (1)$$

where τ_j is the relaxation time for the j th relaxation mode, ϵ_1 ($=\epsilon_s$) is the static dielectric constant, ϵ_j is the dielectric constant associated with the j th relaxation process, ϵ_{∞} is the (extrapolated) dielectric constant at a very high frequency, and m denotes the total number of relaxation modes.

The obtained relaxation time (τ_j) of the water hydrogen bond network in the proximity of membranes was normalized to that of free (bulk) water (i.e., buffer). The concentration-dependent change ($\Delta\tau_j$) in the relaxation time of membrane interfacial water, relative to bulk water, was then fitted to a three-parameter log-normal peak function given by the equation

$$y = a(\exp[-0.5\{\ln(x/x_0)/b\}^2]) \quad (2)$$

where a , b , and x_0 are fitting parameters, with the constraints $x_0 > 0$ and $b > 0$; x and y represent lipid concentration and $\Delta\tau_j$, respectively. In order to delineate the physical significance of the values assigned to each parameter after a fit, [eq 2](#) was simulated by fixing any two of the three parameters and changing values of the third within a physically significant range (see [sections S3 and S4](#) and [Figure S2](#) of the [Supporting Information](#) for more details). Sigma Plot 10.0 (Systat Software Inc., San Jose, CA) was utilized for fitting, analysis, and subsequent plotting of the data.

RESULTS AND DISCUSSION

Lipid vesicles were found to have similar sizes across the concentration range examined, although they appear to be slightly smaller in the case of DOPC/DOPG vesicles (see [section S4](#) and [Figure S1](#)). Time domain and frequency domain THz signals for buffer and lipid vesicles are shown in parts a and b of [Figure 2](#), respectively. The black trace in [Figure 2a](#) shows a representative THz pulse in air. The presence of sample (buffer or lipid vesicles, represented by the other traces in [Figure 2a](#)) in the optical path leads to the reduction in the amplitude of the transmitted THz pulse ($E_{\text{THz}}(t)$), along with a temporal shift. The time domain traces shown in [Figure 2a](#) were converted to the frequency domain ([Figure 2b](#)) by a FFT algorithm for ease of further data analysis. The high signal-to-noise ratio associated with measurements up to ~ 2 THz allowed us to extract optical parameters from the data in the range 0.2–2 THz.

Information on the frequency-dependent absorption coefficient ($\alpha(\nu)$) and refractive index ($n(\nu)$) of the sample is encoded in the changes in amplitude and phase of the transmitted THz pulse, respectively. These optical parameters were determined from the frequency-dependent power and phase of the transmitted pulse and are represented in [Figure 2c](#) and d for vesicles of varying lipid compositions across a concentration range of 0.1–4 mM. The absorption coefficients of lipid vesicles in the THz frequency region correlate to the collective dynamics of water molecules.^{56,57} As shown in the inset of [Figure 2c](#), we found moderate changes in the absorption coefficients in lipid samples (at a representative concentration of 1 mM) relative to that in buffer (bulk water) across the frequency range examined. The change in the absorption coefficient ($\alpha(\nu)$) profile is subtle, yet definite, which distinctly envisages a change in the collective dynamics of water solely in the proximity of lipid vesicles, which indeed

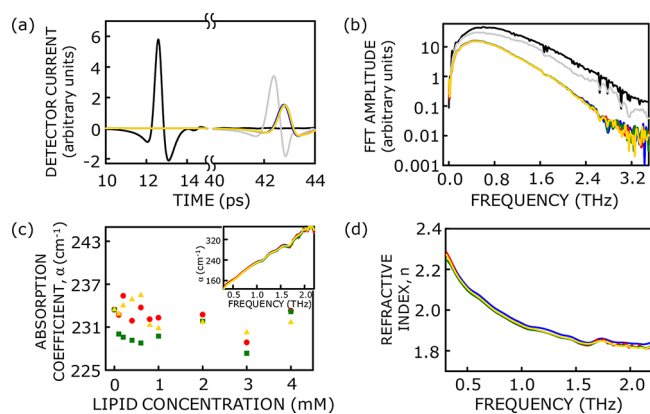


Figure 2. (a) Time domain THz signals and (b) corresponding FFT spectra of dry air (black), empty quartz cell (gray), buffer (blue), and vesicles of DOPC (red), DOPC/DOPG (80/20, mol/mol, green), and DOPC/DOPG (60/40, mol/mol, yellow) at a representative concentration of 1 mM. (c) Concentration-dependent absorption coefficient (α) at 1 THz in vesicles of DOPC (●), DOPC/DOPG (80/20, mol/mol, ■), and DOPC/DOPG (60/40, mol/mol, ▲). Inset shows the frequency dependence of the absorption coefficient (α) of buffer and vesicles of three different lipid compositions at a representative concentration of 1 mM. The color coding is the same as that in part a. (d) Frequency-dependent refractive index (n) of buffer and vesicles of DOPC, DOPC/DOPG (80/20, mol/mol), and DOPC/DOPG (60/40, mol/mol) at a representative concentration of 1 mM. The color coding is the same as that in part a. All experiments were carried out at ~ 20 °C. See the [Experimental Section](#) and the [Supporting Information](#) for more details.

has been confirmed by the dielectric relaxation measurements (see later).

The absorption coefficient ($\alpha(\nu)$) and refractive index ($n(\nu)$) of the samples were utilized to extract the frequency-dependent real (ϵ' or ϵ_{real}), imaginary (ϵ'' or $\epsilon_{\text{imaginary}}$), and complex ($\tilde{\epsilon}$) dielectric constants of the water molecules by simple mathematical equations detailed in [section S1](#). Parts a and b of [Figure 3](#) show the decrease in the real and imaginary dielectric constants of water molecules in the presence of zwitterionic (DOPC) and negatively charged (DOPC/DOPG) lipid vesicles (at a representative concentration of 1 mM) with increasing frequency of the incident THz pulse. This is known as the dielectric relaxation response of water and reflects the reorientation dynamics associated with the permanent dipoles of water molecules in a given sample. In physical terms, an electric field applied to water molecules would induce an alignment of the water dipoles and give rise to an induced polarization proportional to the applied electric field. The induced polarization is quantified by the dispersion amplitude (S_j)

$$S_j = \epsilon_j - \epsilon_{j+1} \quad (3)$$

where ϵ_j is the dielectric constant associated with the j th relaxation process. In the case of an oscillating electric field, the water molecules continually reorient themselves along the applied field, provided the frequency of the applied electric field is slower than the water reorientation frequency. However, once the frequency of the applied field increases above the characteristic reorientation frequency of the water molecules, alignment of the water dipoles along the applied electric field becomes increasingly improbable and leads to a decrease in the induced polarization.

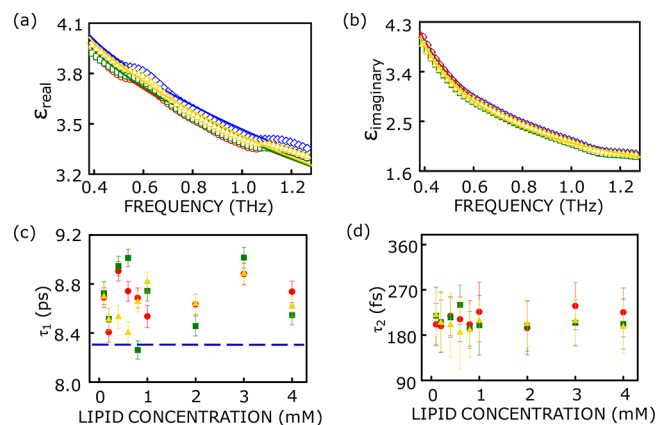


Figure 3. Frequency-dependent (a) real and (b) imaginary dielectric constants of buffer (◇) and vesicles of DOPC (○), DOPC/DOPG (80/20, mol/mol, □), and DOPC/DOPG (60/40, mol/mol, △) at a representative lipid concentration of 1 mM. The solid lines represent fits to the three-exponential Debye model (eq 4). Concentration-dependent Debye relaxation time constants (c) τ_1 and (d) τ_2 of interfacial water in vesicles of DOPC (●), DOPC/DOPG (80/20, mol/mol, ■), and DOPC/DOPG (60/40, mol/mol, ▲). The dashed line in part c represents the Debye relaxation time constant τ_1 of buffer (bulk water). Data shown are representative of at least three independent measurements. See the [Supporting Information](#) for more details.

In general, the frequency-dependent changes in water dielectric constants in the low frequency regime are governed by dielectric relaxation, whereas intermolecular and intramolecular vibrational modes contribute predominantly at higher frequencies.^{45,54} We modeled the dielectric relaxation of water in proximity to lipid vesicles by introducing the three-exponential Debye model,⁵⁵ which describes the frequency-dependent complex permittivity, $\tilde{\epsilon}(\omega)$, as

$$\tilde{\epsilon}(\omega) = \epsilon_{\infty} + \frac{S_1}{1 + i\omega\tau_1} + \frac{S_2}{1 + i\omega\tau_2} + \frac{S_3}{1 + i\omega\tau_3} \quad (4)$$

where S_j is the dispersion amplitude (relaxation strength) of the j th mode ($j = 1, 2, 3$) and ω is the associated angular frequency ($2\pi\nu$).

Frequency-dependent real (ϵ' or ϵ_{real}) and imaginary (ϵ'' or $\epsilon_{\text{imaginary}}$) dielectric constants extracted from the data (see [Figure 3a](#) and [b](#)) were utilized to derive the complex dielectric constant (eq S4), which was fitted to the triple Debye model (eq 4). The fitting parameters are shown in [Tables S1–S3](#). A good fit of experimental data with the three-exponential Debye model indicates that lipid membranes could be represented by three different modes of dielectric relaxation of water molecules, characterized by distinct relaxation time scales. Our analysis yielded time scales of 8.3 ps, 192 fs, and 74 fs for buffer (bulk water), in good agreement with our previous results.⁵⁸ The ~ 8 ps time scale is related to the cooperative reordering of the water hydrogen bond network involving the concerted breaking and reforming of hydrogen bonds through a jump mechanism. The 192 fs time scale originates from the quick jump motion of under-coordinated water molecules, and the 74 fs time scale corresponds to the bending of hydrogen bonds and propagation of transverse acoustic phonons in an orthogonal direction with respect to hydrogen bonds between two neighboring water molecules.^{47,59,60} It is to be noted here that there could be “irrotational” water molecules present in our system, which are so strongly bound that their relaxation

(reorientation) rates are reduced enough to render them invisible to the THz spectral window.⁴⁵

Parts c and d of Figure 3 show the change in the relaxation time associated with the first (τ_1) and second (τ_2) dielectric relaxation modes with lipid concentration for zwitterionic and negatively charged lipid vesicles. The dashed line in Figure 3c represents the characteristic τ_1 for bulk water hydrogen bond reorganization and is known as the Debye time.⁴⁵ Since no appreciable change was observed in the relaxation time scales associated with the second (τ_2) relaxation mode with lipid concentration (see Figure 3d and Tables S1–S3), we focused on exploring the physical implications of the concentration-dependent “rise and dip” signature of the relaxation time (τ_1) associated with the cooperative hydrogen bond reorganization of water molecules in the vicinity of lipid vesicles of differential surface charge (the third (τ_3) mode was kept constant during the fitting to the Debye relaxation model).

For this, we normalized the values of τ_1 for lipid vesicles of each concentration to the value in buffer by subtraction. The normalized plots showing the change in the hydrogen bond reorganization time scales ($\Delta\tau_1$) with lipid concentration for each lipid composition are shown in Figure 4. Visual inspection of each data set revealed the presence of two critical lipid concentrations ($\Delta\tau_{1,\max}^I$ and $\Delta\tau_{1,\max}^{II}$, respectively) at which $\Delta\tau_1$ values peaked (see Figure 4). The data sets were then

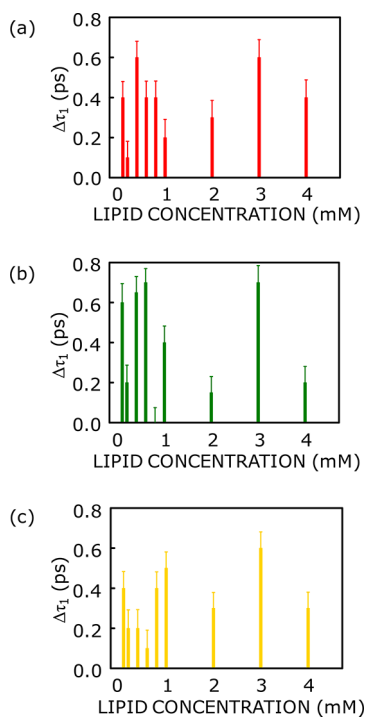


Figure 4. Concentration-dependent changes in Debye relaxation time constant ($\Delta\tau_1$) relative to that of bulk water (represented by the dashed line in Figure 3c) for vesicles of (a) DOPC, (b) DOPC/DOPG (80/20, mol/mol), and (c) DOPC/DOPG (60/40, mol/mol). $\Delta\tau_1$ exhibits an initial increase with lipid concentration, until a critical value ($\Delta\tau_{1,\max}^I$, see Figure 5a), beyond which there is a decrease. The critical lipid concentration corresponding to this inflection point (C_t^I , see Figure 5a) depends on the charge of the lipid headgroup, thereby implying the role of surface electrostatics in structuring the water hydrogen bond network in the proximity of membranes. Data shown are representative of at least three independent measurements. See text for more details.

segregated into two regimes, and regime I (corresponding to lipid concentrations of 0.1–2 mM, see Figure 5a) was subjected to fitting to the asymmetric peak function shown in eq 2. Regime II (corresponding to lipid concentrations of 2–4 mM, see Figure 5a) was not subjected to data fitting due to the lack of statistical robustness associated with fitting three data points to a three-parameter equation. A good fit was defined as one

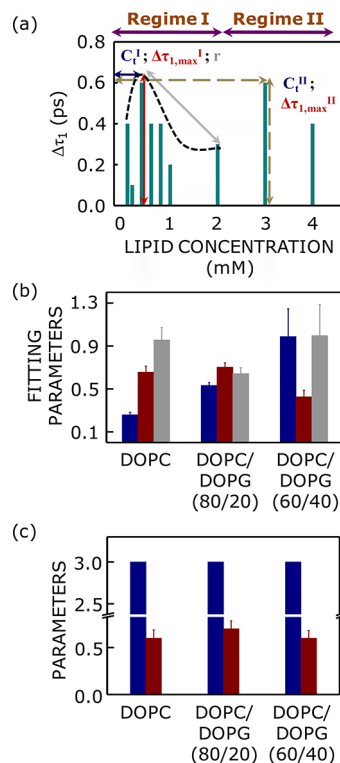


Figure 5. (a) Representative schematic showing the parameters extracted upon fitting the concentration-dependent changes in relaxation time constant ($\Delta\tau_1$) for DOPC vesicles (data from Figure 4a) to the log-normal asymmetric function (eq 2). Only data points in regime I (corresponding to lipid concentrations of 0.1–2 mM) were subjected to the fit. The parameters extracted (x_o , a , and b) are shown as blue, maroon, and gray solid arrows, respectively. As shown in Figure S2, x_o denotes the critical lipid concentration (C_t^I) corresponding to maximum $\Delta\tau_1$ ($\Delta\tau_{1,\max}^I$; given by a), beyond which there is a decrease in the relaxation time. The extent of decrease in the relaxation time (and overall order in the water hydrogen bond network) as a consequence of crowding is given by r and is inversely proportional to b . Regime II, consisting of only three data points (corresponding to lipid concentrations of 2–4 mM), was not subjected to fitting, and the values for C_t^{II} and the corresponding $\Delta\tau_{1,\max}^{II}$ (shown as brown dashed arrows) were obtained solely by visual inspection. (b) Phospholipid headgroup dependence of the parameters obtained by fitting the data points in regime I (corresponding to lipid concentrations of 0.1–2 mM, see part a) from Figure 4 to eq 2. The extracted fitting parameters C_t^I , $\Delta\tau_{1,\max}^I$, and r are represented as blue, maroon, and gray bars, respectively. Data shown are representative of at least three independent measurements. (c) Phospholipid headgroup dependence of the critical lipid concentration, C_t^{II} , and the corresponding $\Delta\tau_{1,\max}^{II}$ in regime II (corresponding to lipid concentrations of 2–4 mM) of the data shown in Figure 4. Regime II, consisting of only the last three data points, was not fitted to eq 2, and the values reported here were obtained solely by visual inspection. The color coding is the same as that in part a. See the Experimental Section and the Supporting Information for more details.

with $R^2 \geq 0.9$. Other details of the fitting method employed are described in section S2. Fitting with eq 2 yielded lipid composition dependent values of the three floating parameters involved (denoted as a , b , and x_c), which are shown in Figure 5b. In order to delineate the physical significance of the values assigned to each floating parameter and the observed changes with lipid composition, eq 2 was analytically simulated with appropriate constraints (see section S3 for further details).

The analytically simulated plots (see Figure S2) show that x_c represents the critical lipid concentration (C_t) corresponding to the maximum $\Delta\tau_1$. The parameter a is directly proportional to the height of the distribution and denotes the maximum increase in the hydrogen bond reorganization time scales ($\Delta\tau_{1,\max}$). This is directly proportional to the extent of membrane-induced ordering of water molecules, which leads to a decrease in the reorientation rate. The floating parameter b is inversely proportional to the decrease of $\Delta\tau_{1,\max}$ (and $\tau_{1,\max}$) beyond the critical lipid concentration and represents the loss (r) of overall order in the water hydrogen bond network induced by increasing lipid concentration.

In general, the inclusion of membranes resulted in an increase in τ_1 (Figure 3c). This implies an increased residence time of water at the membrane interface. This could be attributed to an induction of stronger ordering (or stabilization of the hydrogen bond network) of water due to the charged membrane interface. However, as Figure 4 shows, $\Delta\tau_1$ decreases again beyond a certain lipid concentration, and the inflection point (lipid concentration) appears to depend on the membrane composition (fraction of negatively charged lipids present). This could be explained by the following scenario. While each vesicle orders water molecules around it isotropically, the average residence time of a single hydrogen bond between a water molecule and the membrane interface decreases due to the cumulative anisotropic ordering of water molecules by several neighboring vesicles (due to crowding at higher lipid concentrations). Such a type of lipid crowding could be relevant in the context of cellular hydration. Interestingly, such ordering of water in the proximity of membranes has been previously reported for simulated membrane–water interfaces,⁶¹ reverse micelles,⁶² supported bilayers,⁴⁵ and stacked bilayers.²⁸

The lipid concentration (in mM) corresponding to the maximum increase in reorientation time of membrane interfacial water (C_t^I , see Figure 5a) increases linearly with increasing mole percent of negatively charged DOPG (blue bars in Figure 5b). This could be due to stronger repulsive (electrostatic) forces between the negatively charged DOPC/DOPG membrane interfaces, relative to the zwitterionic DOPC interface. In addition, a negatively charged interface would induce stronger hydrogen bonds with water molecules and, consequently, the stronger hydrogen bond network would require greater crowding (achieved at higher lipid concentrations) in order to be destabilized.

The height of the distribution (a) represents the extent of water ordering induced by proximity to the membrane interface at the critical lipid concentration ($\Delta\tau_{1,\max}^I$ in ps, see Figure 5a). We found $\Delta\tau_{1,\max}^I$ to be constant for DOPC and DOPC/DOPG (80/20, mol/mol) vesicles at a value of ~ 0.7 ps and was reduced to ~ 0.4 ps in the case of DOPC/DOPG (60/40, mol/mol) vesicles (maroon bars in Figure 5b). These changes assume significance, since the sensitivity of the experimental setup employed is of the order of 0.1 ps. The width of the distribution (b) is inversely proportional to the loss of ordering

in the hydration sheath beyond the critical lipid concentration. This appears to be minimum (~ 0.6) for DOPC/DOPG (80/20, mol/mol) vesicles and increases to a value of ~ 1 for both DOPC and DOPC/DOPG (60/40, mol/mol) (gray bars in Figure 5b). It is to be noted that the analysis employed here yields information on the extent of water ordering and the loss of overall order only at and beyond the critical lipid concentration (C_t^I) which is appreciably different for the three lipid compositions used. The parameters, $\Delta\tau_{1,\max}^I$ and r , would therefore be influenced by lipid composition and concentration.

The extent of water hydrogen bond stabilization (in terms of its relaxation time, $\Delta\tau_{1,\max}^I$, maroon bars in Figure 5b) induced by DOPC at a concentration of 0.3 mM (C_t^I for DOPC) is similar to that observed in DOPC/DOPG (80/20, mol/mol) at a much higher concentration (0.7 mM; C_t^I for DOPC/DOPG (80/20, mol/mol)). Since greater surface charge (corresponding to more negatively charged lipid content) should induce higher ordering of water in the vicinity, this seems counter-intuitive. The decrease in $\Delta\tau_{1,\max}^I$ (~ 0.4 ps) for DOPC/DOPG (60/40, mol/mol) vesicles could be due to the disordering effect associated with steric crowding that dominates over the ordering influence of increased surface (negative) charge. A similar reasoning may be invoked for the largest disorder induced by the membrane interface in DOPC/DOPG (80/20, mol/mol) vesicles, where weaker electrostatic repulsions (relative to DOPC/DOPG (60/40, mol/mol) vesicles) ensure a closer approach between neighboring vesicles (see gray bars in Figure 5b) and manifest as a strong dependence on crowding.

We observed a repetition of the “rise and dip” trend in Debye relaxation times with lipid concentration in regime II (see Figure 4 and Figure 5a). At this point in time, the reason for this type of behavior is not clear. Interestingly, the parameters for regime II (critical lipid concentration, C_t^{II} , and the maximum increase in water relaxation time scale, $\Delta\tau_{1,\max}^{II}$) shown in Figure 5c do not show any lipid composition dependent changes. This could imply that, at lipid concentrations beyond 2 mM, the extent of crowding is the predominant determinant of water hydrogen bond structure and there is negligible dependence on lipid composition. Taken together, our results show that the critical lipid concentration (C_t^I), the maximum water reorientation time ($\Delta\tau_{1,\max}^I$) corresponding to C_t^I , and the loss (r) of order in the water hydrogen bond network with lipid concentration beyond the inflection point (C_t^I) depend on the charge of the lipid headgroup in a concentration-dependent fashion.

CONCLUSION

In this work, we have explored the microstructure and collective dynamics of the extended hydration shell associated with zwitterionic and negatively charged phospholipid membrane bilayers using THz-TDS. Our results show that the cooperative relaxation time constants of the water hydrogen bond network show a unique “rise and dip” variation with lipid concentration (Figure 4). In addition, the critical lipid concentration corresponding to the inflection point was found to depend on the charge of the lipid headgroup (see Figure 6), thereby implicating membrane electrostatics as a major governing factor in the microstructure and dynamics of water at the membrane interface. To the best of our knowledge, our results constitute one of the first reports on the modulation of the dielectric relaxation response of membrane interfacial

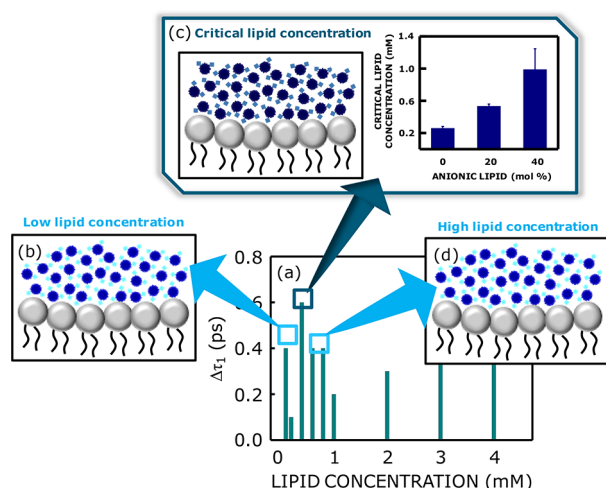


Figure 6. Schematic representation of the effect of phospholipid headgroup charge on the microstructure and dynamics of water at the membrane interface. Panel a shows a representative “rise and dip” trend of relaxation time constants with lipid concentration (see Figure 5a). Membrane interfacial water molecules with lower relaxation time constants (and faster hydrogen bond reorganization) are shown in light blue (panels b and d), and those with higher relaxation time constants (and slower hydrogen bond reorganization) are shown in dark blue (panel c). The relaxation time constant is maximum at the critical lipid concentration (C_t^1) and decreases both before and after C_t^1 . The critical lipid concentration corresponding to this inflection point depends on the charge of the lipid headgroup, thereby implicating membrane electrostatics as a major governing factor in the dynamics of water at the membrane interface. These results have important implications for understanding the regulation of a variety of membrane-associated phenomena by diverse membrane lipids in the cellular context. See text for more details.

water by lipid composition in a concentration-dependent manner. These observations gain importance in the context of emerging evidence on the crucial role of water dynamics in various membrane associated phenomena, such as the function of ion channels²⁴ and the activation of membrane receptors.^{20,63,64} In addition, this lipid-stringent membrane hydration assumes relevance in the global context of the lipid diversity observed in biological membranes³⁶ and the regulatory role of negatively charged lipids in membrane protein structure^{65,66} and function.^{37–39,67–69} We envision that these results would contribute toward developing a comprehensive framework for understanding the regulation of a variety of membrane-associated phenomena by diverse membrane lipids in a biological milieu.

■ ASSOCIATED CONTENT

Supporting Information

The Supporting Information is available free of charge on the ACS Publications website at DOI: 10.1021/acs.jpcc.8b01633.

Section S1, extraction of THz-TDS optical parameters; section S2, fitting of experimental data to the asymmetric log-normal peak function; section S3, analytical simulation of the log-normal peak function; section S4, determination of vesicle size; Tables S1–S3, concentration-dependent Debye relaxation fitting parameters for interfacial water in vesicles of DOPC, DOPC/DOPG (80/20), and DOPC/DOPG (60/40), respectively; Figure S1, concentration-dependent vesicle size in DOPC, DOPC/DOPG (80/20), and DOPC/DOPG

(60/40) membranes; Figure S2, analytical simulation of the log-normal peak function (PDF)

■ AUTHOR INFORMATION

Corresponding Authors

*E-mail: rajib@bose.res.in. Phone: 033-2335-5706.

*E-mail: amit@ccmb.res.in. Phone: 040-2719-2578.

ORCID

Sreetama Pal: 0000-0002-7153-1402

Nirnay Samanta: 0000-0002-5746-6907

Rajib Kumar Mitra: 0000-0001-9159-0517

Amitabha Chattopadhyay: 0000-0002-2618-2565

Author Contributions

[†]S.P., N.S.: Equal contribution.

Notes

The authors declare no competing financial interest.

■ ACKNOWLEDGMENTS

This work was supported by the Council of Scientific and Industrial Research, Govt. of India (A.C.). R.K.M. acknowledges funding from 12th Five Year Plan project at SNBNCBS (SNB/AB/12-13/96) and Department of Science and Technology, Govt. of India (SB/S1/PC-056/2013). A.C. gratefully acknowledges support from J.C. Bose Fellowship (Department of Science and Technology, Govt. of India). S.P. thanks the University Grants Commission (India) for the award of a Senior Research Fellowship. A.C. is an Adjunct Professor of Tata Institute of Fundamental Research (Mumbai), RMIT University (Melbourne, Australia), Indian Institute of Technology (Kanpur), and Indian Institute of Science Education and Research (Mohali). We thank Dr. HIRAK Chakraborty for help with planning preliminary experiments, and members of the Chattopadhyay laboratory for their comments and discussions.

■ REFERENCES

- (1) Bao, G.; Suresh, S. Cell and Molecular Mechanics of Biological Materials. *Nat. Mater.* **2003**, *2*, 715–725.
- (2) Pal, S.; Chattopadhyay, A. What Is So Unique About Biomembrane Organization and Dynamics? In *Membrane Organization and Dynamics*; Chattopadhyay, A., Ed.; Springer: Heidelberg, Germany, 2017; pp 1–9.
- (3) Budin, I.; Szostak, J. W. Expanding Roles for Diverse Physical Phenomena During the Origin of Life. *Annu. Rev. Biophys.* **2010**, *39*, 245–263.
- (4) Tanford, C. The Hydrophobic Effect and the Organization of Living Matter. *Science* **1978**, *200*, 1012–1018.
- (5) Israelachvili, J. N.; Marčelja, S.; Horn, R. G. Physical Principles of Membrane Organization. *Q. Rev. Biophys.* **1980**, *13*, 121–200.
- (6) Haldar, S.; Chaudhuri, A.; Chattopadhyay, A. Organization and Dynamics of Membrane Probes and Proteins Utilizing the Red Edge Excitation Shift. *J. Phys. Chem. B* **2011**, *115*, 5693–5706.
- (7) Haldar, S.; Kombrabail, M.; Krishnamoorthy, G.; Chattopadhyay, A. Depth-Dependent Heterogeneity in Membranes by Fluorescence Lifetime Distribution Analysis. *J. Phys. Chem. Lett.* **2012**, *3*, 2676–2681.
- (8) White, S. H.; Wimley, W. C. Membrane Protein Folding and Stability: Physical Principles. *Annu. Rev. Biophys. Biomol. Struct.* **1999**, *28*, 319–365.
- (9) Ashcroft, R. G.; Coster, H. G. L.; Smith, J. R. The Molecular Organisation of Bimolecular Lipid Membranes. The Dielectric Structure of the Hydrophilic/Hydrophobic Interface. *Biochim. Biophys. Acta, Biomembr.* **1981**, *643*, 191–204.

- (10) El-Sayed, M. Y.; DeBose, C. D.; Coury, L. A.; Roberts, M. F. Sensitivity of Phospholipase C (*Bacillus cereus*) Activity to Phosphatidylcholine Structural Modifications. *Biochim. Biophys. Acta, Lipids Lipid Metab.* **1985**, *837*, 325–335.
- (11) Damodaran, S. Water at Biological Phase Boundaries: Its Role in Interfacial Activation of Enzymes and Metabolic Pathways. *Subcell. Biochem.* **2015**, *71*, 233–261.
- (12) Dufresne, M. B.; Petrou, V. I.; Clarke, O. B.; Mancia, F. Structural Basis for Catalysis at the Membrane-water Interface. *Biochim. Biophys. Acta, Mol. Cell Biol. Lipids* **2017**, *1862*, 1368–1385.
- (13) Marrink, S.-J.; Tieleman, D. P.; van Buuren, A. R.; Berendsen, H. J. C. Membranes and Water: an Interesting Relationship. *Faraday Discuss.* **1996**, *103*, 191–201.
- (14) Yeagle, P. *The Membranes of Cells*; Academic Press: Cambridge, MA, 2016; pp 147–148.
- (15) Boggs, J. M. Lipid Intermolecular Hydrogen Bonding: Influence on Structural Organization and Membrane Function. *Biochim. Biophys. Acta, Rev. Biomembr.* **1987**, *906*, 353–404.
- (16) Shin, T.-B.; Leventis, R.; Silvius, J. R. Partitioning of Fluorescent Phospholipid Probes between Different Bilayer Environments. Estimation of the Free Energy of Interlipid Hydrogen Bonding. *Biochemistry* **1991**, *30*, 7491–7497.
- (17) Stubbs, C. D.; Ho, C.; Slater, S. J. Fluorescence Techniques for Probing Water Penetration into Lipid Bilayers. *J. Fluoresc.* **1995**, *5*, 19–28.
- (18) Ho, C.; Slater, S. J.; Stubbs, C. D. Hydration and Order in Lipid Bilayers. *Biochemistry* **1995**, *34*, 6188–6195.
- (19) Disalvo, E. A. Membrane Hydration: A Hint to a New Model for Biomembranes. *Subcell. Biochem.* **2015**, *71*, 1–16.
- (20) Angel, T. E.; Chance, M. R.; Palczewski, K. Conserved Waters Mediate Structural and Functional Activation of Family A (Rhodopsin-like) G Protein-coupled Receptors. *Proc. Natl. Acad. Sci. U. S. A.* **2009**, *106*, 8555–8560.
- (21) Xu, F.; Cross, T. A. Water: Foldase Activity in Catalyzing Polypeptide Conformational Rearrangements. *Proc. Natl. Acad. Sci. U. S. A.* **1999**, *96*, 9057–9061.
- (22) Halder, S.; Chattopadhyay, A. Hydration Dynamics of Probes and Peptides in Captivity. In *Reviews in Fluorescence 2010*; Geddes, C. D., Ed.; Springer: New York, 2012; pp 155–172.
- (23) Chattopadhyay, A.; Halder, S. Dynamic Insight into Protein Structure Utilizing Red Edge Excitation Shift. *Acc. Chem. Res.* **2014**, *47*, 12–19.
- (24) Chaudhuri, A.; Chattopadhyay, A. Molecular Anatomy of an Ion Channel Explored Utilizing Fluorescence Spectroscopy. In *Reviews in Fluorescence 2015*; Geddes, C. D., Ed.; Springer: Heidelberg, Germany, 2016; pp 353–367.
- (25) Crowe, J. H.; Crowe, L. M.; Chapman, D. Infrared Spectroscopic Studies on Interactions of Water and Carbohydrates with a Biological Membrane. *Arch. Biochem. Biophys.* **1984**, *232*, 400–407.
- (26) Kundu, A.; Blasiak, B.; Lim, J.-H.; Kwak, K.; Cho, M. Water Hydrogen-Bonding Network Structure and Dynamics at Phospholipid Multibilayer Surface: Femtosecond Mid-IR Pump-Probe Spectroscopy. *J. Phys. Chem. Lett.* **2016**, *7*, 741–745.
- (27) Tristram-Nagle, S. Use of X-Ray and Neutron Scattering Methods with Volume Measurements to Determine Lipid Bilayer Structure and Number of Water Molecules/Lipid. *Subcell. Biochem.* **2015**, *71*, 17–43.
- (28) Yamada, T.; Takahashi, N.; Tominaga, T.; Takata, S.-I.; Seto, H. Dynamical Behavior of Hydration Water Molecules between Phospholipid Membranes. *J. Phys. Chem. B* **2017**, *121*, 8322–8329.
- (29) Beard, M. C.; Turner, G. M.; Schmuttenmaer, C. A. Terahertz Spectroscopy. *J. Phys. Chem. B* **2002**, *106*, 7146–7159.
- (30) Ferguson, B.; Zhang, X.-C. Materials for Terahertz Science and Technology. *Nat. Mater.* **2002**, *1*, 26–33.
- (31) Plusquellic, D. F.; Siegrist, K.; Heilweil, E. J.; Esenturk, O. Applications of Terahertz Spectroscopy in Biosystems. *ChemPhysChem* **2007**, *8*, 2412–2431.
- (32) Yang, X.; Zhao, X.; Yang, K.; Liu, Y.; Liu, Y.; Fu, W.; Luo, Y. Biomedical Applications of Terahertz Spectroscopy and Imaging. *Trends Biotechnol.* **2016**, *34*, 810–824.
- (33) Ebbinghaus, S.; Kim, S. J.; Heyden, M.; Yu, X.; Heugen, U.; Gruebele, M.; Leitner, D. M.; Havenith, M. An Extended Dynamical Hydration Shell Around Proteins. *Proc. Natl. Acad. Sci. U. S. A.* **2007**, *104*, 20749–20752.
- (34) Meister, K.; Ebbinghaus, S.; Xu, Y.; Duman, J. G.; DeVries, A.; Gruebele, M.; Leitner, D. M.; Havenith, M. Long-range Protein-water Dynamics in Hyperactive Insect Antifreeze Proteins. *Proc. Natl. Acad. Sci. U. S. A.* **2013**, *110*, 1617–1622.
- (35) Hishida, M.; Tanaka, K. Long-range Hydration Effect of Lipid Membrane Studied by Terahertz Time-domain Spectroscopy. *Phys. Rev. Lett.* **2011**, *106*, 158102.
- (36) van Meer, G.; de Kroon, A. I. P. M. Lipid map of the Mammalian Cell. *J. Cell Sci.* **2011**, *124*, 5–8.
- (37) Resh, M. D. Myristylation and Palmitoylation of Src Family Members: The Fats of the Matter. *Cell* **1994**, *76*, 411–413.
- (38) Murray, D.; Arbuzova, A.; Hangyás-Mihályné, G.; Gambhir, A.; Ben-Tal, N.; Honig, B.; McLaughlin, S. Electrostatic Properties of Membranes Containing Acidic Lipids and Adsorbed Basic Peptides: Theory and Experiment. *Biophys. J.* **1999**, *77*, 3176–3188.
- (39) Ghosh, A. K.; Rukmini, R.; Chattopadhyay, A. Modulation of Tryptophan Environment in Membrane-Bound Melittin by Negatively Charged Phospholipids: Implications in Membrane Organization and Function. *Biochemistry* **1997**, *36*, 14291–14305.
- (40) Baron, C. B.; Coburn, R. F. Comparison of Two Copper Reagents for Detection of Saturated and Unsaturated Neutral Lipids by Charring Densitometry. *J. Liq. Chromatogr.* **1984**, *7*, 2793–2801.
- (41) McClare, C. W. F. An Accurate and Convenient Organic Phosphorus Assay. *Anal. Biochem.* **1971**, *39*, 527–530.
- (42) MacDonald, R. C.; MacDonald, R. I.; Menco, B. Ph. M.; Takeshita, K.; Subbarao, N. K.; Hu, L.-R. Small-volume Extrusion Apparatus for Preparation of Large, Unilamellar Vesicles. *Biochim. Biophys. Acta, Biomembr.* **1991**, *1061*, 297–303.
- (43) Polley, D.; Ganguly, A.; Barman, A.; Mitra, R. K. Polarizing Effect of Aligned Nanoparticles in Terahertz Frequency Region. *Opt. Lett.* **2013**, *38*, 2754–2756.
- (44) Polley, D.; Patra, A.; Mitra, R. K. Dielectric Relaxation of the Extended Hydration Sheath of DNA in the THz Frequency Region. *Chem. Phys. Lett.* **2013**, *586*, 143–147.
- (45) Tielrooij, K. J.; Paparo, D.; Piatkowski, L.; Bakker, H. J.; Bonn, M. Dielectric Relaxation Dynamics of Water in Model Membranes Probed by Terahertz Spectroscopy. *Biophys. J.* **2009**, *97*, 2484–2492.
- (46) Choi, D.-H.; Son, H.; Jung, S.; Park, J.; Park, W.-Y.; Kwon, O. S.; Park, G.-S. Dielectric Relaxation Change of Water upon Phase Transition of a Lipid Bilayer Probed by Terahertz Time Domain Spectroscopy. *J. Chem. Phys.* **2012**, *137*, 175101.
- (47) Kindt, J. T.; Schmuttenmaer, C. A. Far-infrared Dielectric Properties of Polar Liquids Probed by Femtosecond Terahertz Pulse Spectroscopy. *J. Phys. Chem.* **1996**, *100*, 10373–10379.
- (48) Nandi, N.; Bagchi, B. Dielectric Relaxation of Biological Water. *J. Phys. Chem. B* **1997**, *101*, 10954–10961.
- (49) Venables, D. S.; Schmuttenmaer, C. A. Far-infrared Spectra and Associated Dynamics in Acetonitrile-water Mixtures Measured with Femtosecond THz Pulse Spectroscopy. *J. Chem. Phys.* **1998**, *108*, 4935–4944.
- (50) Venables, D. S.; Schmuttenmaer, C. A. Spectroscopy and Dynamics of Mixtures of Water with Acetone, Acetonitrile, and Methanol. *J. Chem. Phys.* **2000**, *113*, 11222–11236.
- (51) Yada, H.; Nagai, M.; Tanaka, K. Origin of the Fast Relaxation Component of Water and Heavy Water Revealed by Terahertz Time-domain Attenuated Total Reflection Spectroscopy. *Chem. Phys. Lett.* **2008**, *464*, 166–170.
- (52) Ronne, C.; Thrane, L.; Åstrand, P.-O.; Wallqvist, A.; Mikkelsen, K. V.; Keiding, S. R. Investigation of the Temperature Dependence of Dielectric Relaxation in Liquid Water by THz Reflection Spectroscopy and Molecular Dynamics Simulation. *J. Chem. Phys.* **1997**, *107*, 5319–5331.

- (53) Sato, T.; Buchner, R. Dielectric Relaxation Processes in Ethanol/Water Mixtures. *J. Phys. Chem. A* **2004**, *108*, 5007–5015.
- (54) Møller, U.; Cooke, D. G.; Tanaka, K.; Jepsen, P. U. Terahertz Reflection Spectroscopy of Debye Relaxation in Polar Liquids. *J. Opt. Soc. Am. B* **2009**, *26*, A113–A125.
- (55) van der Post, S. T.; Tielrooij, K.-J.; Hunger, J.; Backus, E. H. G.; Bakker, H. J. Femtosecond Study of the Effects of Ions and Hydrophobes on the Dynamics of Water. *Faraday Discuss.* **2013**, *160*, 171–189.
- (56) Heyden, M.; Havenith, M. Combining THz Spectroscopy and MD Simulations to Study Protein-hydration Coupling. *Methods* **2010**, *52*, 74–83.
- (57) Heyden, M.; Sun, J.; Funkner, S.; Mathias, G.; Forbert, H.; Havenith, M.; Marx, D. Dissecting the THz Spectrum of Liquid Water from First Principles via Correlations in Time and Space. *Proc. Natl. Acad. Sci. U. S. A.* **2010**, *107*, 12068–12073.
- (58) Samanta, N.; Mahanta, D. D.; Mitra, R. K. Collective Hydration Dynamics of Guanidinium Chloride Solutions and its Possible Role in Protein Denaturation: A Terahertz Spectroscopic Study. *Phys. Chem. Chem. Phys.* **2014**, *16*, 23308–23315.
- (59) Walrafen, G. E. Raman Spectral Studies of the Effects of Urea and Sucrose on Water Structure. *J. Chem. Phys.* **1966**, *44*, 3726–3727.
- (60) Vij, J. K.; Simpson, D. R. J.; Panarina, O. E. Far Infrared Spectroscopy of Water at Different Temperatures: GHz to THz Dielectric Spectroscopy of Water. *J. Mol. Liq.* **2004**, *112*, 125–135.
- (61) Marrink, S.-J.; Berkowitz, M.; Berendsen, H. J. C. Molecular Dynamics Simulation of a Membrane/Water Interface: The Ordering of Water and Its Relation to the Hydration Force. *Langmuir* **1993**, *9*, 3122–3131.
- (62) Verma, P. K.; Saha, R.; Mitra, R. K.; Pal, S. K. Slow Water Dynamics at the Surface of Macromolecular Assemblies of Different Morphologies. *Soft Matter* **2010**, *6*, 5971–5979.
- (63) Yuan, S.; Filipek, S.; Palczewski, K.; Vogel, H. Activation of G-protein-coupled Receptors Correlates with the Formation of a Continuous Internal Water Pathway. *Nat. Commun.* **2014**, *5*, 4733.
- (64) Lee, Y.; Kim, S.; Choi, S.; Hyeon, C. Ultraslow Water-mediated Transmembrane Interactions Regulate the Activation of A_{2A} Adenosine Receptor. *Biophys. J.* **2016**, *111*, 1180–1191.
- (65) van Dalen, A.; Hegger, S.; Killian, J. A.; de Kruijff, B. Influence of Lipids on Membrane Assembly and Stability of the Potassium Channel KcsA. *FEBS Lett.* **2002**, *525*, 33–38.
- (66) Betaneli, V.; Petrov, E. P.; Schwill, P. The Role of Lipids in VDAC Oligomerization. *Biophys. J.* **2012**, *102*, 523–531.
- (67) de Vrije, T.; de Swart, R. L.; Dowhan, W.; Tommassen, J.; de Kruijff, B. Phosphatidylglycerol is Involved in Protein Translocation across *Escherichia coli* Inner Membranes. *Nature* **1988**, *334*, 173–175.
- (68) Jordan, P.; Fromme, P.; Witt, H. T.; Klukas, O.; Saenger, W.; Krauß, N. Three-dimensional Structure of Cyanobacterial Photosystem I at 2.5 Å Resolution. *Nature* **2001**, *411*, 909–917.
- (69) Valiyaveetil, F. I.; Zhou, Y.; MacKinnon, R. Lipids in the Structure, Folding, and Function of the KcsA K⁺ Channel. *Biochemistry* **2002**, *41*, 10771–10777.